UC Berkeley
UC Berkeley Previously Published Works

Title

Metal–Oxygen Hybridization Determined Activity in Spinel-Based Oxygen Evolution Catalysts: A Case Study of ZnFe2–x Cr x O4

Permalink

https://escholarship.org/uc/item/1fp4j8vs

Journal

Chemistry of Materials, 30(19)

ISSN

0897-4756

Authors

Li, Haiyan
Sun, Shengnan
Xi, Shibo
et al.

Publication Date

2018-10-09

DOI

10.1021/acs.chemmater.8b02871

Peer reviewed

Metal-oxygen Hybridization Determined Activity in Spinel-based Oxygen Evolution Catalysts: A Case Study of ZnFe2-xCrxO4

Journal:	*Chemistry of Materials*
Manuscript ID	cm-2018-02871r.R2
Manuscript Type:	Article
Date Submitted by the Author:	12-Sep-2018
Complete List of Authors:	Li, Haiyan; Nanyang Technological University, Materials Science and Engineering Sun, Shengnan; Nanyang Technological University, Materials Science & Engineering Xi, Shibo; Agency for Science, Technology and Research, Chen, YuBo; Nanyang Technological University, School of Materials Science and Engineering Wang, Ting; Nanyang Technological University, Materials Science & Engineering Du, Yonghua; Institute of Chemical and Engineering Sciences, Sherburne, Matthew; University of California, Department of Materials Science and Engineering Ager, Joel; Lawrence Berkeley National Laboratory, Materials Sciences Division Fisher, Adrian; International Research Center for Soft Matter, Beijing University of Chemical Technology, Xu, Zhichuan J.; Nanyang Technological University, Materials Science & Engineering

SCHOLARONE™
Manuscripts

Metal-oxygen Hybridization Determined Activity in Spinel-based Oxygen Evolution Catalysts: A Case Study of ZnFe$_{2-x}$Cr$_x$O$_4$

Haiyan Li,[†,¶]+ Shengnan Sun,[†,¶]+ Shibo Xi,[∥,]* Yubo Chen,[†] Ting Wang,[†] Yonghua Du,[∥]

Matthew Sherburne,[Δ] Joel W. Ager,[Δ] Adrian C. Fisher,[‡] Zhichuan J. Xu[†,¶,§]*

[†]School of Materials Science and Engineering, Nanyang Technological University, 639798, Singapore

[¶]Solar Fuels Laboratory, Nanyang Technological University, 639798, Singapore

[∥]Institute of Chemical and Engineering Sciences A*STAR, 1 Pesek Road, 627833, Singapore

[Δ]Department of Materials Science and Engineering, University of California at Berkeley, Berkeley, California 94720, USA

[‡]Department of Chemical Engineering, University of Cambridge, Cambridge, CB2 3RA, UK

[§]Energy Research Institute @NTU, ERI@N, Interdisciplinary Graduate School, Nanyang Technological University, 639798, Singapore

ABSTRACT:

A good understanding of the correlation between electronic properties and catalytic performance is vital to the rational design of active oxygen evolution reaction (OER) catalysts. Here, a volcano-shaped correlation between the OER activity and Cr substitution amount was found for spinel oxides $ZnFe_{2-x}Cr_xO_4$ (x = 0~2), in which Zn^{2+} resides in tetrahedral (Td) sites while Fe^{3+} and Cr^{3+} occupy octahedral (Oh) sites. Such a relationship probably is because Cr substitution tunes the e_g occupancy of Oh-site transition metals (TM_{Oh}) via the Oh-Oh superexchange effect. Density functional calculations further revealed the hybridization degree between the TM_{Oh} 3d and the O 2p states and a volcano-shaped trend was also found in the variation of TM_{Oh} 3d-O 2p hybridization with the amount of Cr substitution. The good correlation between the OER activity and the hybridization highlights the important role of metal-oxygen hybridization in determining the OER activity of these spinel oxides.

INTRODUCTION

Water electrolysis holds great potential to mass produce renewable hydrogen fuel and thus provides an efficient means to reduce the Earth's reliance on fossil fuels and decrease greenhouse gas emissions.[1] However, its anodic half-reaction, oxygen evolution reaction (OER), has sluggish kinetics, greatly reducing the energy efficiency of the overall reaction. Significant efforts have been made over past decades to develop highly active electrocatalysts to improve the reaction rate of OER.[2-3] Oxides based on noble metals, such as RuO_2 and IrO_2, are the state-of-the art OER catalysts,[4-5] but their scarcity and high price do not allow for a global, large-scale implementation. As an alternative, oxides based on earth-abundant transition metals (TM) are low cost and have demonstrated promising activity, making them attractive for large-scale applications.[6-11]

To accelerate the catalyst screening and rationalize the catalyst design, revealing the intrinsic factors that affect the OER activity of transition metal oxides (TMOs) is the key.[2] Current opinion on efficient OER electrocatalysts is built upon the Sabatier principle that an optimal catalyst should not bind reaction intermediates too strongly nor too weakly.[2, 8, 12] Hence, generally there is a volcano-shaped correlation between catalytic efficiency and the binding strength between catalysts and reactants, with the optimal binding strength determining the peak of the volcano. The difference in the surface electronic structures of catalysts is a vital cause of the diversity of their binding ability (and therefore their catalytic performance).[13] Yet, upon water oxidation, transition-metal oxides are under high anodic potential and thus their electronic properties

3

may dynamically change with the applied potential.[14-18] Currently, two popular methods are employed in OER studies. One is the operando investigation of surface change of oxides under OER conditions.[14-16] The other is the correlation between the electronic structures of oxides and their OER activities.[19] The latter has successfully revealed a few descriptors relevant with the electronic properties of TMOs, such as the number of d electrons,[20] transition-metal e_g filling,[8] metal-oxygen covalency,[21] O 2p-band center,[7] and etc.

Among them, transition-metal e_g filling, together with covalency, works well so far as a descriptor to explain the OER activity trends of TMOs in many perovskite structures.[8] For perovskite-structured TMOs, the octahedrally-coordinated transition-metal cations are the active sites for OER catalysis. Their interaction with oxygenated intermediates greatly depends on the coupling between the transition-metal e_g states and the valence states of the oxygen-related adsorbate. Thus, the e_g filling of transition-metal ions is closely linked to the bond strength between the active sites and the OER intermediates. And a medium level of e_g filling, i.e. an e_g occupancy close to unity, indicates an optimal bond strength and thus a maximum intrinsic OER activity. Moreover, the OER activity can be further enhanced by the increased covalency of the metal-oxygen bond.[8]

Motivated by the effectiveness of e_g-filling descriptor for rationalizing the difference in catalytic performance and designing perovskites with high activity, attempts have been made to utilize it to other structures of TMOs, for instance, spinel, another widely studied family of OER catalysts.[9] Unlike the perovskite structure, in

4

which only octahedral (Oh) interstitials are available for transition metal cations and thus regarded as the OER active sites, the spinel structure provides tetrahedral (Td) and Oh interstitials simultaneously (Figure 1a), which is a more complicated situation. Because Td coordination results in a lower degree of metal-oxygen covalency, Td-site cations are supposed to be much less active than the same element in Oh sites for OER catalysis.[9] On the other hand, the magnetic cations in Td and Oh sites interact via superexchange, which is generally stronger than the Oh-Oh superexchange interaction.[22] Thus, the Td-Oh superexchange interaction has the possibility of positively or negatively affecting the activity of Oh-site cations.
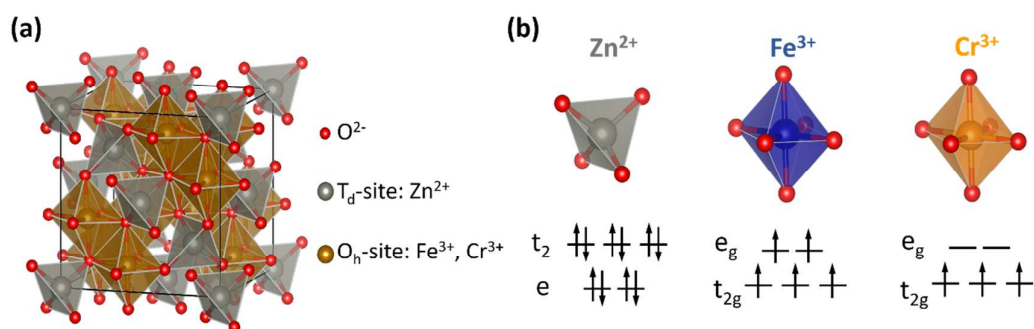
Figure 1. (a) A polyhedral model of spinel oxides, in which the red balls are oxygen anions, gray balls are Td-site cations, and gold balls are Oh-site cations. **(b)** Schematic illustration of the d-orbitals of tetrahedrally-coordinated Zn^{2+}, octahedrally-coordinated Fe^{3+} (HS), and octahedrally-coordinated Cr^{3+} in the spinel structure.

To clarify the role played by Oh-site cations in determining OER activity in spinel structure TMOs, without interference from Td sites, $ZnFe_{2-x}Cr_xO_4$ (x = 0, 0.5, 1, 1.5, 2) TMOs were employed in this study. For the endpoint TMOs, $ZnFe_2O_4$ and

ZnCr$_2$O$_4$ (Figure 1), catalytically inactive Zn^{2+} with d^{10} electronic configuration prefers to occupy Td sites, while Fe^{3+} in the high spin state (HS) or Cr^{3+} mainly resides in Oh sites.[23] And, as shown in Figure 1b, there are two electrons on the e$_g$ orbital of Fe^{3+} (HS) while none on that of Cr^{3+}.[23] Thus, the nominal average e$_g$ number of Oh-site TM cations (TM$_{Oh}$) in ZnFe$_{2-x}$Cr$_x$O$_4$ decreases from 2 to 0 with the increase of Cr substitution. Furthermore, since Zn^{2+} has fully occupied d orbitals, the superexchange interaction between cations in ZnFe$_{2-x}$Cr$_x$O$_4$ primarily occurs between the Oh sites, which may allow for tuning of the electronic configuration of TM$_{Oh}$. The distribution and valence of zinc, iron and chromium cations in ZnFe$_{2-x}$Cr$_x$O$_4$ synthesized by this study are confirmed by X-ray adsorption spectroscopy (XAS) measurement. And with the help of density functional theory calculations (DFT), the correlation between the OER activities and metal-oxygen hybridization in ZnFe$_{2-x}$Cr$_x$O$_4$ is revealed.

EXPERIMENTAL SECTION

Synthesis of ZnFe$_{2-x}$Cr$_x$O$_4$ particles. The synthesis of spinel ZnFe$_{2-x}$Cr$_x$O$_4$ (x = 0, 0.5, 1, 1.5, 2) was accomplished by a low-temperature sol-gel method. All chemicals were obtained from Sigma-Aldrich and used as-is. A mixture of 30 mmol nitrate salts (composed of stoichiometric amounts of Zn(NO$_3$)$_2$•6H$_2$O, Fe(NO$_3$)$_3$•9H$_2$O and Cr(NO$_3$)$_3$•9H$_2$O), 60 mmol citric acid and 30 mmol urea was dissolved in 200 ml de-ionized water (DI water) to form an aqueous solution. After addition of 20 mL nitrite acid, the solution was heated and continuously stirred at 90

□C until a homogeneous gel formed. Then the gel was heated at 170 □C for 12 hours to form the resin, followed by annealing at 800 □C in air for 6 hours.

Material Characterization. A Bruker D8 Advance with Cu Kα radiation (λ = 1.5418 Å) was used to collect the X-ray diffraction (XRD) data of samples. The FESEM images were recorded on a JEOL FESEM 7600F at 5kV. XAS spectra were collected at the XAFCA beamline of the Singapore Synchrotron Light Source.[24] An ASAP Tristar II 3020 was used to measure the Brunauer–Emmett–Teller (BET) specific surface area and the average particle size of samples.

Electrode preparation. Oxide electrodes were prepared by drop-casting the ink of catalysts onto glassy carbon electrodes (GCEs) with the geometric surface area of 0.196 cm^2. Oxides and acetylene black (AB) were dispersed in a solvent consisting of water, isopropanol and Nafion® perfluorinated resin solution (5 wt% in water) to form a 5 mg$_{Oxide}$/mL mixture. The mass ratio of oxides to AB was maintained at 4, and the volume ratio of DI water: isopropanol: Nafion were kept at 4: 1: 0.05. Before drop-casting, GCE were polished with alumina slurry for 30 minutes, cleaned by repeated ultrasonication in ethanol and DI water and finally dried at ambient condition. The mixture was ultrasonicated for 30 minutes to achieve a homogenous dispersion of oxides and AB. Then, the ink was drop-casted and dried at room temperature to evaporate water and IPA. 10 μL ink of ZnFe$_{2-x}$Cr$_x$O$_4$ (x = 0, 0.5, 1, 1.5, 2) was dropped onto GCE, yielding an oxide mass loading of 255.10 μg/cm^2$_{disk}$.

Electrochemical measurement. A three-electrode cell configuration was utilized, consisting of a GC electrode, a platinum sheet and a Hg/HgO (1.0 M KOH)

reference electrode (0.098 V vs. RHE). All cyclic voltammetry (CV) measurements were conducted from 0.8 V to 1.73 V (vs. RHE) at a scan rate of 2 mV s^{-1} in 1.0 M KOH electrolyte. All potentials were referenced to RHE scale and corrected for Ohmic resistance. The resistance was determined by electrochemical impedance spectra (EIS) measurements. All EIS were recorded at 1.53 V (vs. RHE) with frequencies ranging from 10^5 to 10^{-1} Hz and an AC voltage amplitude of 10 mV.

DFT calculations. DFT calculations in this study were performed using the Vienna Ab Initio Simulation Package (VASP) software.[25-26] The interaction between atomic cores and valence electrons was modeled by the projector augmented-wave (PAW) method.[27] The exchange-correlational effects of valence electrons were described by the generalized gradient approximation (GGA) method with a Perdew−Burk−Ernzerhof (PBE) functional.[28] To improve the description of the on-site Coulomb interaction of the transition-metal d electrons, the GGA+U approach was adopted by using the standard Dudarev implementation in VASP. The effective values of U parameters for Zn, Fe and Cr in $ZnFe_{2-x}Cr_xO_4$ (x = 0, 0.5, 1, 1.5, 2) were set to be 7.1, 4.0 and 3.2 eV, respectively, which are taken from literature and have previously been applied to capture the electronic properties of $ZnFe_2O_4$ and $ZnCr_2O_4$.[29] The conventional standard Fd-3m spinel structure was employed as the initial structures of $ZnFe_{2-x}Cr_xO_4$, as shown in Figure 1a. Before the calculation of the electronic density of states (DOS), the cells and atomic positions of these initial structures were fully relaxed, with a 0.02 eV/Å force convergence and a 10^{-6} eV energy tolerance. Subsequently, the ground state electronic properties were computed

using the tetrahedron method with Blöchl corrections.[30] For all calculations, a Γ-centered $5 \times 5 \times 5$ k-point grid was applied and a plane-wave cut-off energy of 520 eV was used.

RESULTS AND DISCUSSION

Material Characterization. As verified by XRD characterization and Rietveld refinement analysis (Figure 2a-e and Table S1), all the as-synthesized $ZnFe_{2-x}Cr_xO_4$ are in a single phase of cubic structure with Fd-3m space group. The results of Rietveld refinement also show that the lattice parameters (a = b = c) of $ZnFe_{2-x}Cr_xO_4$ monotonically decrease with the increase of Cr substitution (Figure 2f). This feature was also reported in previous studies about the crystal structures of $ZnFe_{2-x}Cr_xO_4$ and was attributed to lattice dimension contraction resulted from the smaller radius of Cr^{3+} cations than Fe^{3+} cations in Oh sites.[31-32] The FESEM images of $ZnFe_{2-x}Cr_xO_4$ in Figure S2 display that the variation of Cr content causes little difference in their morphology. This is supported by the only slight differences between the BET specific surface areas of $ZnFe_{2-x}Cr_xO_4$, which are in the same order of magnitude (Figure S2f).
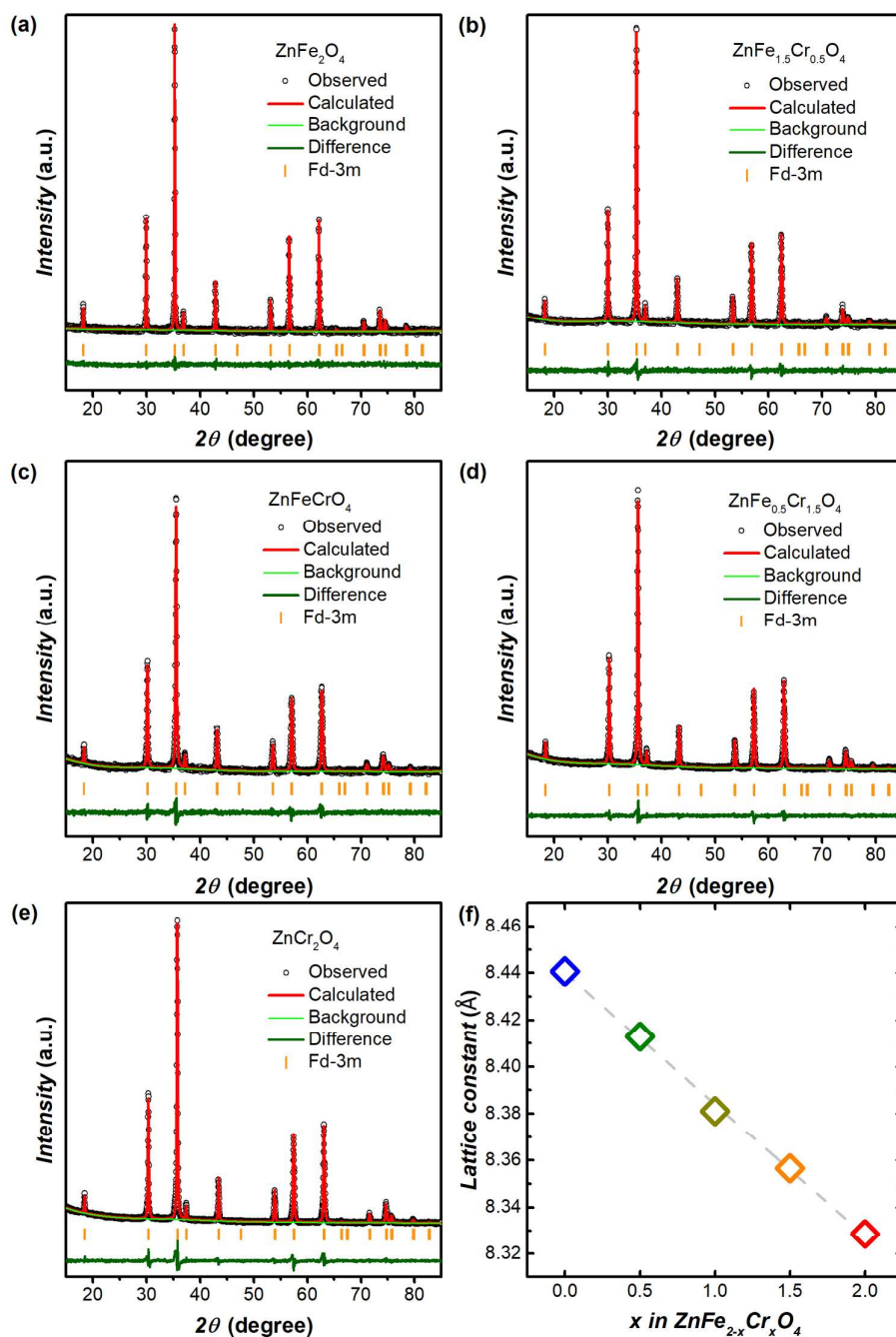
Figure 2. XRD patterns and Rietveld refinement results of as-synthesized **(a)** $ZnFe_2O_4$, **(b)** $ZnFe_{1.5}Cr_{0.5}O_4$, **(c)** $ZnFeCrO_4$, **(d)** $ZnFe_{0.5}Cr_{1.5}O_4$ and **(e)** $ZnCr_2O_4$. **(f)** Evolution of the lattice parameter with the content of Cr substitution.

The valence states of zinc, iron and chromium cations in $ZnFe_{2-x}Cr_xO_4$ were detected by X-ray absorption near-edge spectroscopy (XANES) (Figure 3a-c),

10

according to the shift of the absorption edge of the corresponding element. The edge position is determined as the energy at the highest first derivative of the absorbance, and its movement indicates the variation of oxidation states of the absorbed element. As shown in Figure 3d, there is little fluctuation in the edge positions of $ZnFe_{2-x}Cr_xO_4$, no matter the detected element is Zn, Fe or Cr. Hence, the oxidation states of zinc, iron and chromium cations in $ZnFe_{2-x}Cr_xO_4$ remain largely unchanged with the variation of Cr content.

To further investigate the valence states of Zn, Fe, and Cr in $ZnFe_{2-x}Cr_xO_4$, XPS measurement was conducted. In the Fe 2p XPS spectra (Figure S3). It can be observed that the binding energies for Fe $2p_{1/2}$ and Fe $2p_{3/2}$ are about 724.6 eV and 711.2 eV, respectively. It also can be observed that satellite peaks for Fe $2p_{1/2}$ and Fe $2p_{3/2}$ are located at 732.6 eV and 718.8 eV, respectively. These characteristic structures reveal that the valence state of Fe is 3+.[33-34] In the Cr 2p XPS spectra (Figure S3), the binding energies for Cr $2p_{1/2}$ and Cr $2p_{3/2}$ are around 586.2 eV and 576.5 eV, respectively, supporting that Cr cations are in trivalent state.[35-36] In the XPS spectra of Zn 2p (Figure S4). The two peaks centered at ~1045 and ~1022 eV can be attributed to Zn $2p_{1/2}$ and Zn $2p_{3/2}$, respectively, indicating that Zn cations are in divalent state.[37-38] The above XPS analysis further supports the results of XANES characterization that the oxidation states of Zn, Fe and Cr in $ZnFe_{2-x}Cr_xO_4$ remain largely unchanged with the variation of Cr content.
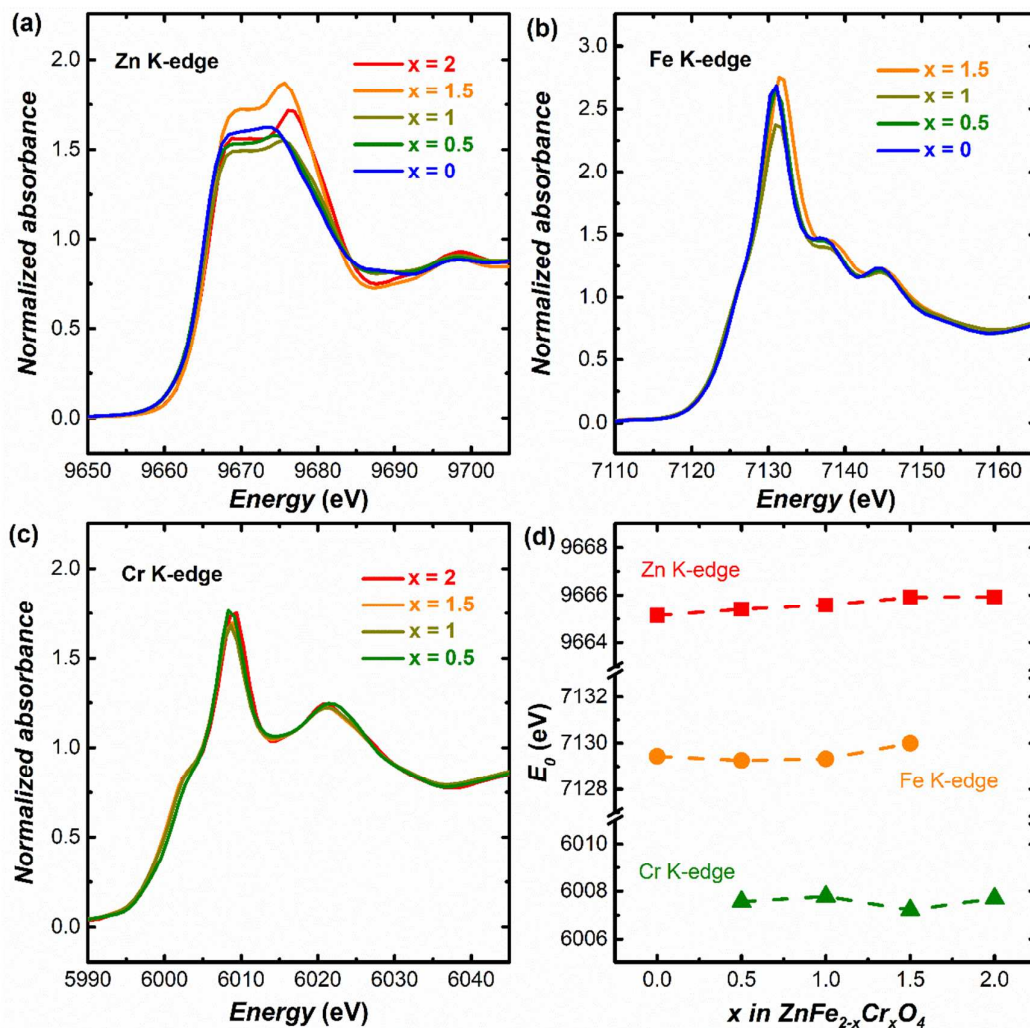
Figure 3. (a-c) Zn K-edge, Fe K-edge and Cr K-edge XANES spectra of ZnFe$_{2-x}$Cr$_x$O$_4$, respectively. **(d)** The edge positions E$_0$ of ZnFe$_{2-x}$Cr$_x$O$_4$ in Zn K-edge, Fe K-edge and Cr K-edge XANES spectra. E$_0$ is set to be the energy at the highest peak of the first derivative of the absorbance, the shift of which can reflect the variation of oxidation states of the absorbing element.

The geometrical occupation information of metal cations in ZnFe$_{2-x}$Cr$_x$O$_4$ synthesized by this study was uncovered by extended X-ray absorption fine-structure spectroscopy (EXAFS). The Fourier transformation (FT) spectra of EXAFS results

can differentiate octahedrally-coordinated cations from tetrahedrally-coordinated by their difference in interatomic distances. Irregardless of whether the absorbing cation is in the Oh or Td site of a spinel, a peak appears at ~1.5Å in the FT spectrum due to the single scattering from its nearest oxygen anions, and a peak emerges at ~3.0 Å because of the scattering from its surrounding metal cations in Oh or Td sites.[39-40] On the other hand, if the absorbing cation is octahedrally coordinated, an additional peak exists at ~2.5 Å, owing to the scattering from its closest Oh-site metal cations.[39] Due to the scattering phase-shift, the interatomic distances observed from a FT spectrum are around 0.5 Å shorter than the real values.[41] As displayed in Figure 4a-c, both iron and chromium ions in $ZnFe_{2-x}Cr_xO_4$ possess two kinds of cation-cation bond distance (of ~2.5 and ~3.0 Å, respectively), whereas zinc ion only has one kind of cation−cation bond distance of ~3.0 Å. In addition, the oxygen coordination number of Zn, Fe, and Cr in $ZnFe_{2-x}Cr_xO_4$ can be determined by EXAFS fitting (details are shown in Figure S5-7 and summarized in Table S2-4). As shown in Figure 4d, Fe and Cr cations are coordinated by six oxygen whereas Zn cations are surrounded by four oxygen anions. Hence, Fe and Cr in bulk $ZnFe_{2-x}Cr_xO_4$ are octahedrally coordinated while Zn cations are tetrahedrally coordinated. Our results agree well with previous EXAFS analysis for bulk $ZnFe_2O_4$ and $ZnCr_2O_4$, which demonstrates that both of them are normal spinel.[42-43] It was also reported in those studies that there is some degree of inversion for nanocrystalline $ZnFe_2O_4$ or $ZnCr_2O_4$, where Zn^{2+} and Fe^{3+}/Cr^{3+} distribute over Td and Oh sites. Yet, $ZnFe_{2-x}Cr_xO_4$ crystals prepared in this study are microparticles with the average particle size of several micrometers (Table

13

S5). Therefore, for $ZnFe_{2-x}Cr_xO_4$ synthesized in this work, iron or chromium cations

mainly reside in Oh sites, and zinc cations in Td sites. Besides, it can be also observed

from Figure 4a-c that the positions of peaks in FT spectra slightly shift with the

variation of Cr content. This probably results from the contraction of the lattice when

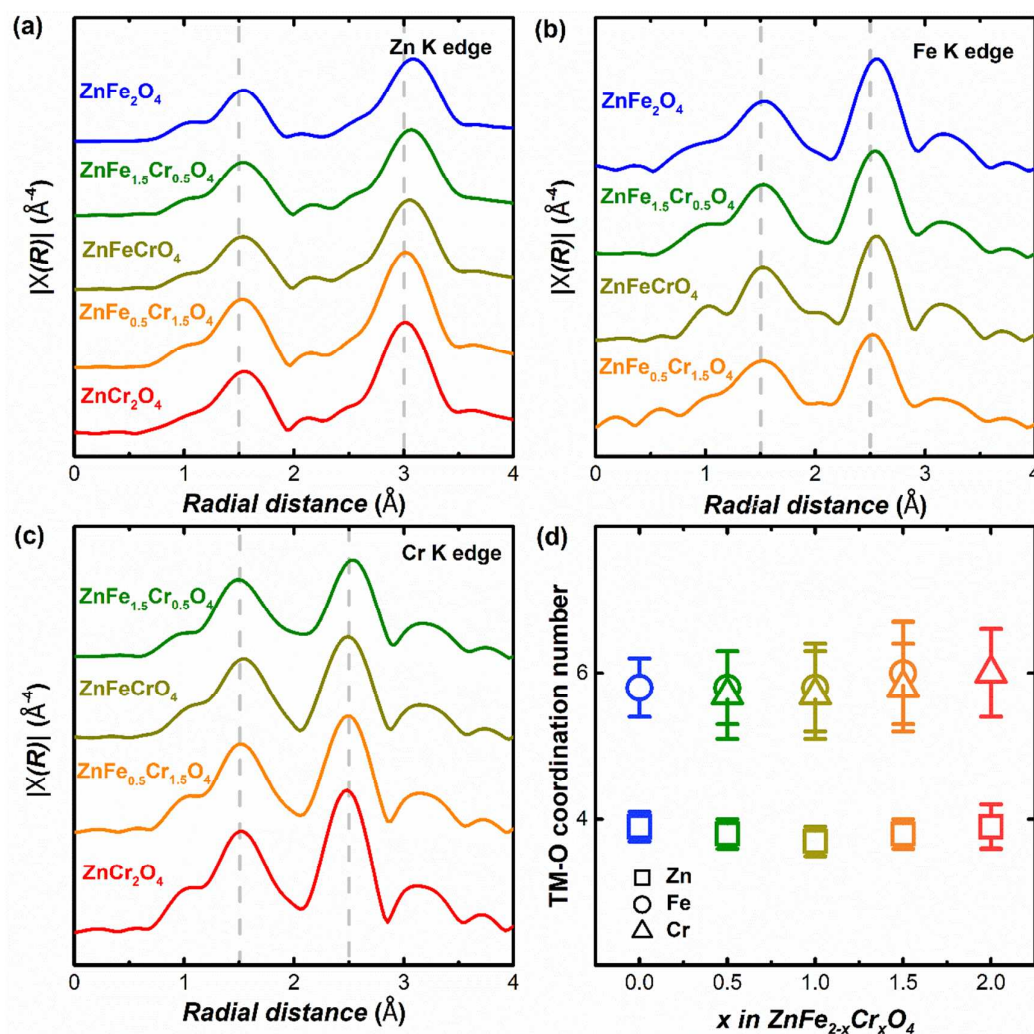iron cations in octahedral sites are replaced by smaller chromium cations.

Figure 4. (a-c) The Fourier transforms of Zn K-edge, Fe K-edge and Cr K-edge

EXAFS spectra of $ZnFe_{2-x}Cr_xO_4$, respectively, which are not corrected for the

scattering phase-shift. The dashed gray lines in (a-c) are used to indicate the peaks

arising from atomic scattering. **(d)** TM-O (TM = Zn, Fe, and Cr) coordination number in $ZnFe_{2-x}Cr_xO_4$.

The above XAS results agrees well with our expectation that Fe^{3+} and Cr^{3+} stay in Oh sites while Zn^{2+} remain in Td sites of $ZnFe_{2-x}Cr_xO_4$. Earlier work states that Fe^{3+} cations in Oh sites in zinc spinel oxides are in the HS state.[23] This is consistent with our XRD results that the increase of Cr/Fe ratio in $ZnFe_{2-x}Cr_xO_4$ causes the decrease of lattice constant because of the lager cation size of Oh-site Fe^{3+} than Oh-site Cr^{3+}. According to the revised ionic radii published by Shannon,[44] the cation size follows the order of Fe^{3+} (HS) > Cr^{3+} > Fe^{3+} (LS) (Table S6). Hence, the Fe^{3+} in $ZnFe_{2-x}Cr_xO_4$ tested here should be in the HS state and thus have e_g occupancy of two.

Electrochemical Characterization. To exclude the effect of surface area, the intrinsic OER activities of $ZnFe_{2-x}Cr_xO_4$ were obtained by normalizing the results of CV scans to their real surface area determined by BET approach. As shown in the normalized CV curves (Figure 5a), an anodic redox peak for $ZnCr_2O_4$, attributed to the oxidation of Cr(III) to Cr(VI), appears at around 1.30 V (anodic) vs. RHE.[45] As more Cr is incorporated into $ZnFe_2O_4$, this characteristic feature gradually rises and the capacitive current before the onset of OER also increases. The correlation between the Cr(III)/Cr(VI) redox peak and Cr content in $ZnFe_{2-x}Cr_xO_4$ suggests that the Fe/Cr ratio on the surface follows that of the bulk.

15

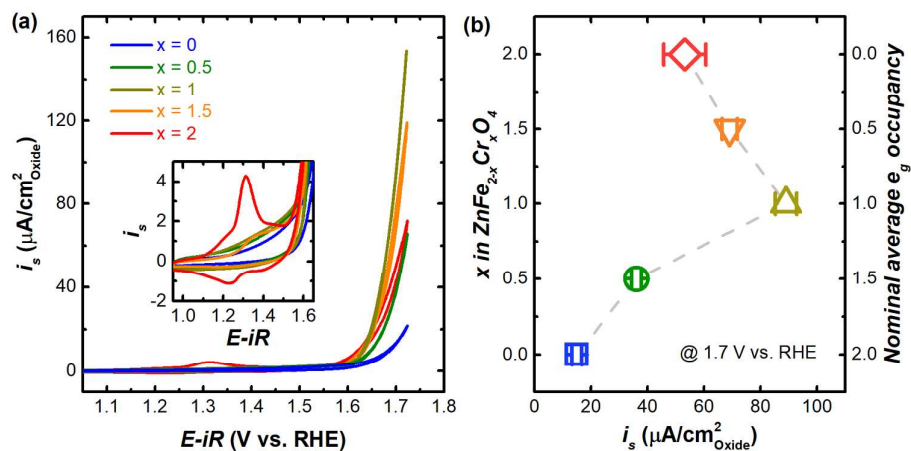**Figure 5. (a)** CV curves (from 1.05 - 1.75 V vs. RHE) of $ZnFe_{2-x}Cr_xO_4$ in 1 M KOH

solution at a scan rate of 2 mV s^{-1}. The inset displays the Cr(III)/Cr(VI) redox peaks

in the CV curves of $ZnFe_{2-x}Cr_xO_4$. All the curves are corrected for Ohmic resistance.

(b) Evolution of the specific OER activity (at 1.7 V vs. RHE) of $ZnFe_{2-x}Cr_xO_4$ with

the content of Cr substitution (left y axis) and the nominal average e_g occupancy of

Oh-site cations (right y axis). Error bars represent standard deviation of at least three

measurements.

   To compare the OER catalytic performance of $ZnFe_{2-x}Cr_xO_4$, their specific activities

at 1.7 V vs. RHE were extracted and plotted in Figure 5b. The variation of the OER

activity with the Cr content in $ZnFe_{2-x}Cr_xO_4$ follows a volcano trend with a peak at x

equals one. This volcano trend in activity may arise from the variation in the e_g filling

of Oh-site cations (right y-axis, Figure 5b). The e_g occupancy of Oh-site Fe^{3+} (HS)

and Oh-site Cr^{3+} is 2 and 0, respectively. Thus, the nominal average e_g filling of

Oh-site cations in $ZnFe_{2-x}Cr_xO_4$ decreases from 2 to 0 with the increase of Cr doping.

When the Fe/Cr ratio is 1: 1, the nominal average e_g number of Oh-site cations is

unity and the activity is the highest. This is consistent with previous reports that too

16

much or too little eg filling impedes OER catalysis.[8-9] The tuning effect on e_g number is possibly due to the superexchange interaction between Oh-site cations. Because Zn^{2+} has completely filled the d orbitals, the superexchange interaction between Oh and Td sites is should be negligible, whereas the Oh-Oh electronic interaction may transfer e_g electrons from Fe to Cr. Although the electronic structure of $ZnFeCrO_4$ is optimized, the OER activity of $ZnFeCrO_4$ (1.68 V vs. RHE @ 50 μA cm_{Oxide}^{-2}) is not competitive enough when compared to those perovskites with e_g occupancy close to unity.[8] This may be resulted from that the actual tuning effect by Cr substitution on the e_g filling of $ZnFe_2O_4$ is limited.

DFT calculation. The lattice parameters of $ZnFe_{2-x}Cr_xO_4$ optimized by DFT calculation match well with the experimental values determined by Rietveld analysis (Figure S8). As found in past studies, the lattice parameters computed by the GGA + U method are slightly higher than the experimental ones (by less than 2%).[46-47] To analyze the electronic properties of $ZnFe_{2-x}Cr_xO_4$, density of states (DOS) calculations were performed on the DFT optimized structures. The partial DOS (PDOS) plots of Zn 3d, Fe 3d, Cr 3d, and O 2p orbitals for $ZnFe_{2-x}Cr_xO_4$ are displayed in Figure S9. It is clear that the DOS at the Fermi energy E_F is empty and their band gaps (summarized in Table S7) are within 3 eV, which is in agreement with previous DFT+U studies[29, 48] and experiments[49-51]. The DFT calculated band gaps of $ZnFe_{2-x}Cr_xO_4$ (summarized in Table S7) are different from each other, indicating the difference in their conductivity. The OER activities of $ZnFe_{2-x}Cr_xO_4$ are plotted as a function of their band gaps, as shown in Figure S10. And no correlation is found

between catalytic activity and band gaps. It implies that the conductivity may not be the variable for the activity of $ZnFe_{2-x}Cr_xO_4$ catalysts. This is consistent with what have been widely reported in oxide catalysts. The possible reason is that the electrons do not need to go through oxide particles within the catalyst composite (oxides mixed with carbon) and thus the intrinsic conductivity of oxides is not influential.[51] In Figure S9, it is also observable that the states close to the Fermi energy are dominated by O 2p states as well as Fe/Cr 3d states while the d electrons of Zn (located 7-9 eV below E_F) contribute little to the top valence band. States around the Fermi level are considered to play an important role in binding the reaction intermediates.[52] Therefore, the interaction between O 2p-band and TM_{Oh} (i.e. Fe or Cr) 3d-band is the key for determining the OER activities of $ZnFe_{2-x}Cr_xO_4$, whereas Td-site Zn cations are ineffective for electrocatalysis. Besides, it can be found that the features of Fe 3d-band are gradually weak while those of Cr 3d-band gradually become strong with the increase of Cr substitution. Hence, to properly analyze the effect of TM_{Oh}-O electronic interactions, the PDOS of Fe 3d-band are superposed with that of Cr 3d-band, as shown in Figure 6a.
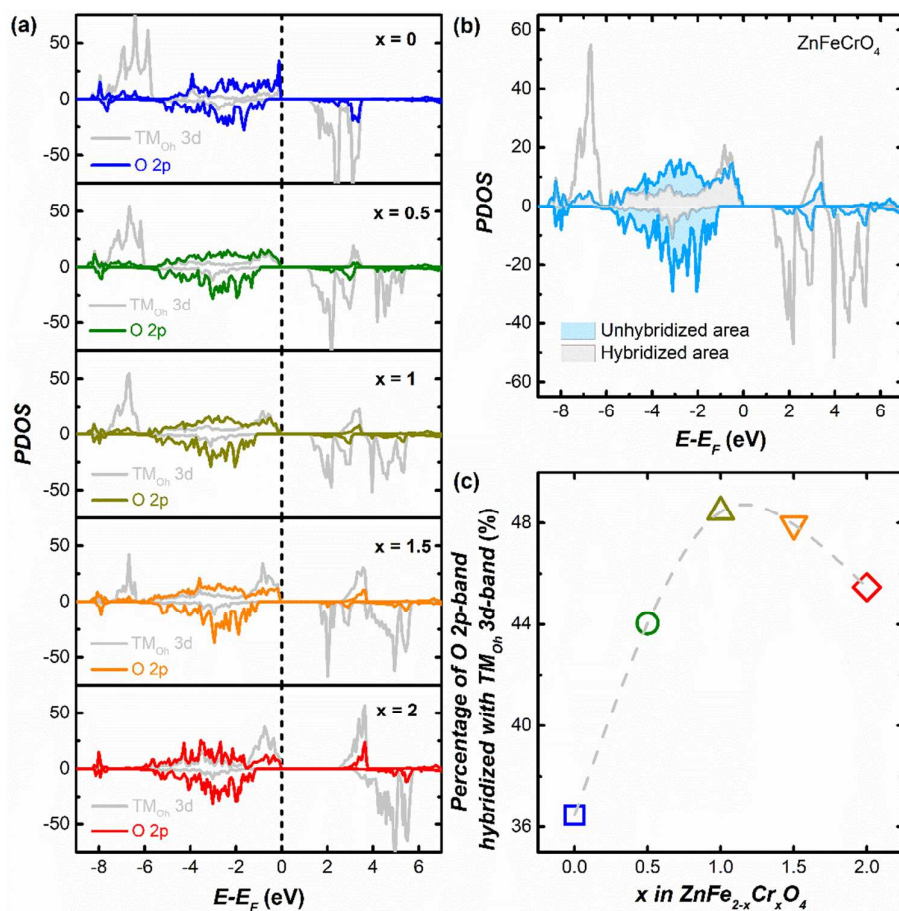
Figure 6. (a) DFT calculated PDOS plots of TM_{Oh} 3d and O 2p orbitals for

$ZnFe_{2-x}Cr_xO_4$. For $ZnFe_{2-x}Cr_xO_4$ (x = 0.5, 1 and 1.5), the gray lines are the

superposition of Fe and Cr 3d DOS. The energy of Fermi level is set to be zero. **(b)**

Illustration for computing the percentage of O 2p states that hybridize with TM_{Oh} 3d

states. The gray shaded area shows the overlapped bands and the light blue shaded

area represents the O 2p-bands unassociated with the hybridization. **(c)**

Volcano-shaped trend in the hybridization intensity of $ZnFe_{2-x}Cr_xO_4$. The intensity is

estimated according to the percentage of O 2p-band hybridized with TM_{Oh} 3d-band.

The dashed gray line is shown to indicate the trend.

Previous research on TMOs with high OER activity highlights the importance of the hybridization between TM 3d and O 2p states.[6, 8, 10] And TMOs with increased hybridization are expected to have increased metal-oxygen covalency and thus enhanced OER activity.[21] As illustrated in Figure 6b, the overlapping area of O 2p-band and TM_{Oh} 3d-band indicates the hybridization between the two bands. The higher the degree of the overlap is, the stronger the hybridization is. To assess the intensity of hybridization for $ZnFe_{2-x}Cr_xO_4$, the percentage of O 2p states mixing with TM_{Oh} 3d states is used as an indicator. As Figure 6b displays, the gray shaded area represents the O 2p orbitals overlapped with TM_{Oh} 3d orbitals, while the light blue shaded area corresponds to the O 2p states unassociated with the hybridization. Thus, the sum of the two kinds of area approximately equals to the overall O 2p states. When the hybridization degree increases with the overlapped bands, the proportion of O 2p orbitals associated with hybridization is also expected to be enhanced. The evolution of the hybridization parameter for $ZnFe_{2-x}Cr_xO_4$ with chromium content are shown in Figure 6c. As the gray dashed line indicates, the hybridization intensity of $ZnFe_{2-x}Cr_xO_4$ follows a volcano-shaped trend, and that of $ZnFeCrO_4$ is at the peak. Therefore, Cr substitution tunes not only the e_g filling of TM_{Oh} cations but also the TM_{Oh} 3d-O 2p hybridization of $ZnFe_{2-x}Cr_xO_4$. In addition, with the increase of Cr substitution, the intensity of Fe 3d-O 2p hybridization almost linearly decreases while that of Cr 3d-O 2p hybridization increases (Figure S11). This correlation suggests that both Fe and Cr cations in $ZnFe_{2-x}Cr_xO_4$ are active sites for OER catalysis.

The classical OER mechanism (as shown in Figure 7a) is centered on surface transition-metal cation redox chemistry and involves four coupled electron-proton transfer steps.[53-54] Recently, a few reports demonstrate that the OER mechanisms are dependent on the bulk electronic structure of perovskites.[55-56] Increasing the covalency of metal-oxygen bonds may enable the participation of lattice oxygen oxidation in the OER, and the OER mechanism involving lattice-oxygen oxidation is fundamentally different form the traditional one.[55] However, as displayed in Figure 6a, the O 2p-band centers of $ZnFe_{2-x}Cr_xO_4$ lie far below the Fermi level, which indicates the inactivation of lattice oxygen redox reactions during the OER.[55] Hence, the trend of OER kinetics observed for $ZnFe_{2-x}Cr_xO_4$ should be explained by the traditional concerted proton-electron transfer mechanism on TM_{Oh} cation sites. For the conventional OER mechanism, the fast OER kinetic is expected to be originated from an optimal binding strength between the OER intermediates and surface metal cations.[8, 54] It is proposed that too much eg filling impedes O−O bond formation at metal sites, while too little hampers the detachment of proton from surface oxyhydroxide.[8] Therefore, the e_g filling of TM_{Oh} cations tuned due to the substitution of Cr into $ZnFe_2O_4$ probably varies the OER activity of the TM_{Oh} cations. Furthermore, it is found that greater covalency of TM-O bonds promotes the OER kinetics on the surface metal sites.[8] As displayed in Figure 7b, the hybridization intensities of $ZnFe_{2-x}Cr_xO_4$ are positively correlated with their specific activities, which agrees with previous reports that stronger metal-oxygen hybridization is critical to the oxygen electrocatalytic activity.[8, 21, 57] The positive correlation between the

hybridization and the OER activity is attributed to that the increased hybridization reflects the reduced energy difference between TM 3d and O 2p states (i.e. higher TM-O covalency),[21] which accelerates the rate of charge transfer between the TM cations and the OER intermediates, and thus positively affects the OER activity.
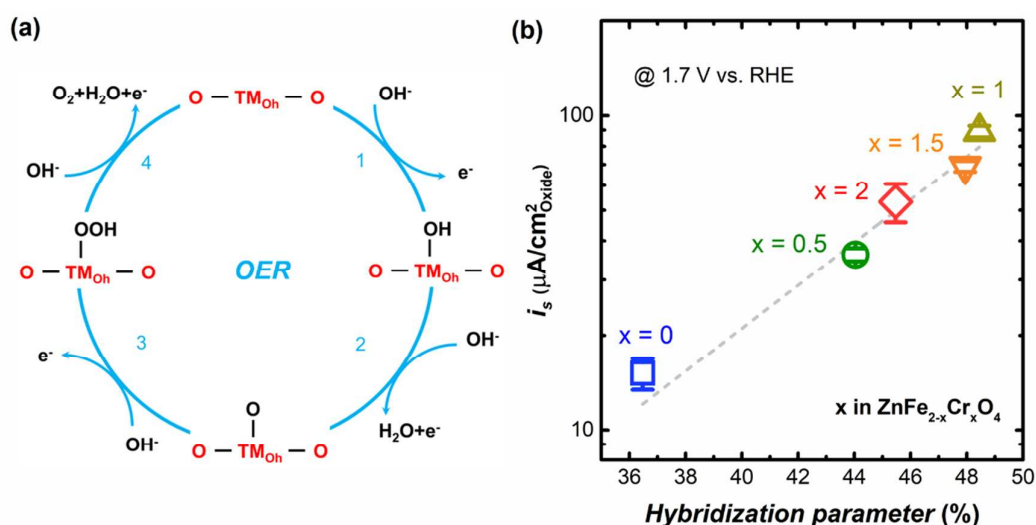

Figure 7. (a) Illustration of the classical OER mechanism involving four concerted proton-electron transfer steps. **(b)** Correlation of the specific OER activity with the TM_{oh}-O hybridization intensity, indicating that the enhanced TM_{oh}-O hybridization trends with the increased OER activity. Error bars represent standard deviation of at least three measurements.

Conclusions

In this study, our electrochemical results show that the intrinsic OER activities of $ZnFe_{2-x}Cr_xO_4$ follow a volcano relation with Cr content and reach the highest as the Fe/Cr ratio is 1. That is attributed to superexchange interactions between Oh-site cations, i.e. Fe and Cr, which tunes their e_g filling despite limited tuning effect. In

addition, the gradual substitution of Fe by Cr also alters the hybridization degree of the TM_{Oh} 3d-O 2p states in $ZnFe_{2-x}Cr_xO_4$, in view of the volcano-shaped trend in the hybridization parameters that are obtained from DFT calculation. And it was also found that the TM_{Oh} 3d-O 2p hybridization intensity in $ZnFe_{2-x}Cr_xO_4$ is positively correlated to their OER activities, which further confirms the important role of metal-oxygen hybridization in the design of active OER catalysts.

ASSOCIATED CONTENT

Supporting Information. BET characterizations, SEM figures, DFT analysis, and tables are included in the Supporting Information. This material is available free of charge via the Internet at http://pubs.acs.orgs.

AUTHOR INFORMATION

Corresponding Authors

*E-mail: xuzc@ntu.edu.sg; xi_shibo@nus.edu.sg

Author Contributions

[+]These authors contributed equally. The manuscript was written through contributions of all authors. All authors have given approval to the final version of the manuscript.

ACKNOWLEDGMENTS

REFERENCES

1. Lewis, N. S.; Nocera, D. G., Powering the Planet: Chemical Challenges in Solar Energy Utilization. *P Natl Acad Sci USA* **2006**, *103*, 15729-15735.

2. Hong, W. T.; Risch, M.; Stoerzinger, K. A.; Grimaud, A.; Suntivich, J.; Shao-Horn, Y., Toward the Rational Design of Non-Precious Transition Metal Oxides for Oxygen Electrocatalysis. *Energ Environ Sci* **2015**, *8*, 1404-1427.

3. Suen, N. T.; Hung, S. F.; Quan, Q.; Zhang, N.; Xu, Y. J.; Chen, H. M., Electrocatalysis for the Oxygen Evolution Reaction: Recent Development and Future Perspectives. *Chem Soc Rev* **2017**, *46*, 337-365.

4. Lee, Y.; Suntivich, J.; May, K. J.; Perry, E. E.; Shao-Horn, Y., Synthesis and Activities of Rutile IrO$_2$ and RuO$_2$ Nanoparticles for Oxygen Evolution in Acid and Alkaline Solutions. *J Phys Chem Lett* **2012**, *3*, 399-404.

5. McCrory, C. C. L.; Jung, S. H.; Peters, J. C.; Jaramillo, T. F., Benchmarking Heterogeneous Electrocatalysts for the Oxygen Evolution Reaction. *J Am Chem Soc* **2013**, *135*, 16977-16987.

6. Duan, Y.; Sun, S. N.; Xi, S. B.; Ren, X.; Zhou, Y.; Zhang, G. L.; Yang, H. T.; Du, Y. H.; Xu, Z. C. J., Tailoring the Co 3d-O 2p Covalency in $LaCoO_3$ by Fe Substitution to Promote Oxygen Evolution Reaction. *Chem Mater* **2017**, *29*, 10534-10541.

7. Grimaud, A.; May, K. J.; Carlton, C. E.; Lee, Y. L.; Risch, M.; Hong, W. T.; Zhou, J. G.; Shao-Horn, Y., Double Perovskites as a Family of Highly Active Catalysts for Oxygen Evolution in Alkaline Solution. *Nat Commun* **2013**, *4*, 2439.

8. Suntivich, J.; May, K. J.; Gasteiger, H. A.; Goodenough, J. B.; Shao-Horn, Y., A Perovskite Oxide Optimized for Oxygen Evolution Catalysis from Molecular Orbital Principles. *Science* **2011**, *334*, 1383-1385.

9. Wei, C.; Feng, Z. X.; Scherer, G. G.; Barber, J.; Shao-Horn, Y.; Xu, Z. C. J., Cations in Octahedral Sites: A Descriptor for Oxygen Electrocatalysis on Transition-Metal Spinels. *Adv Mater* **2017**, *29*, 1606800.

10. Yagi, S., et al., Covalency-Reinforced Oxygen Evolution Reaction Catalyst. *Nat Commun* **2015**, *6*, 8249.

11. Zhu, Y. L.; Zhou, W.; Chen, Y. B.; Yu, J.; Liu, M. L.; Shao, Z. P., A High-Performance Electrocatalyst for Oxygen Evolution Reaction: $LiCo_{0.8}Fe_{0.2}O_2$. *Adv Mater* **2015**, *27*, 7150-7155.

12. Burke, M. S.; Zou, S. H.; Enman, L. J.; Kellon, J. E.; Gabor, C. A.; Pledger, E.; Boettcher, S. W., Revised Oxygen Evolution Reaction Activity Trends for First-Row Transition-Metal (Oxy)Hydroxides in Alkaline Media. *J Phys Chem Lett* **2015**, *6*, 3737-3742.

13. Norskov, J. K.; Bligaard, T.; Rossmeisl, J.; Christensen, C. H., Towards the Computational Design of Solid Catalysts. *Nat Chem* **2009**, *1*, 37-46.

14. Tung, C. W.; Hsu, Y. Y.; Shen, Y. P.; Zheng, Y. X.; Chan, T. S.; Sheu, H. S.; Cheng, Y. C.; Chen, H. M., Reversible Adapting Layer Produces Robust Single-Crystal Electrocatalyst for Oxygen Evolution. *Nat Commun* **2015**, *6*, 8106.

15. Hsu, C. S.; Suen, N. T.; Hsu, Y. Y.; Lin, H. Y.; Tung, C. W.; Liao, Y. F.; Chan, T. S.; Sheu, H. S.; Chend, S. Y.; Chen, H. M., Valence- and Element-Dependent Water Oxidation Behaviors: In Situ X-Ray Diffraction, Absorption and Electrochemical Impedance Spectroscopies. *Phys Chem Chem Phys* **2017**, *19*, 8681-8693.

16. Fabbri, E., et al., Dynamic Surface Self-Reconstruction Is the Key of Highly Active Perovskite Nano-Electrocatalysts for Water Splitting. *Nat Mater* **2017**, *16*, 925-931.

17. Hung, S. F.; Hsu, Y. Y.; Chang, C. J.; Hsu, C. S.; Suen, N. T.; Chan, T. S.; Chen, H. M., Unraveling Geometrical Site Confinement in Highly Efficient Iron☐Doped Electrocatalysts toward Oxygen Evolution Reaction. *Advanced Energy Materials* **2018**, *8*, 1701686.

18. May, K. J.; Carlton, C. E.; Stoerzinger, K. A.; Risch, M.; Suntivich, J.; Lee, Y.-L.; Grimaud, A.; Shao-Horn, Y., Influence of Oxygen Evolution During Water Oxidation on the Surface of Perovskite Oxide Catalysts. *The journal of physical chemistry letters* **2012**, *3*, 3264-3270.

19. Hong, W. T.; Welsch, R. E.; Shao-Horn, Y., Descriptors of Oxygen-Evolution Activity for Oxides: A Statistical Evaluation. *J Phys Chem C* **2016**, *120*, 78-86.

20. Calle-Vallejo, F.; Inoglu, N. G.; Su, H. Y.; Martinez, J. I.; Man, I. C.; Koper, M. T. M.; Kitchin, J. R.; Rossmeisl, J., Number of Outer Electrons as Descriptor for Adsorption Processes on Transition Metals and Their Oxides. *Chem Sci* **2013**, *4*, 1245-1249.

21. Suntivich, J.; Hong, W. T.; Lee, Y. L.; Rondinelli, J. M.; Yang, W. L.; Goodenough, J. B.; Dabrowski, B.; Freeland, J. W.; Shao-Horn, Y., Estimating Hybridization of Transition Metal and Oxygen States in Perovskites, from O K-edge X-ray Absorption Spectroscopy. *J Phys Chem C* **2014**, *118*, 1856-1863.

22. Bercoff, P. G.; Bertorello, H. R., Exchange Constants and Transfer Integrals of Spinel Ferrites. *J Magn Magn Mater* **1997**, *169*, 314-322.

26

23. Murata, T.; Kozuka, Y.; Uchida, M.; Kawasaki, M., Magnetic Properties of Spin Frustrated Spinel $ZnFe_2O_4/ZnCr_2O_4$ Superlattices. *J Appl Phys* **2015**, *118*.

24. Du, Y. H.; Zhu, Y.; Xi, S. B.; Yang, P.; Moser, H. O.; Breese, M. B. H.; Borgna, A., XAFCA: A New XAFS Beamline for Catalysis Research. *J Synchrotron Radiat* **2015**, *22*, 839-843.

25. Kresse, G.; Furthmuller, J., Efficient Iterative Schemes for Ab Initio Total-Energy Calculations Using a Plane-Wave Basis Set. *Phys Rev B* **1996**, *54*, 11169-11186.

26. Kresse, G.; Furthmuller, J., Efficiency of Ab-Initio Total Energy Calculations for Metals and Semiconductors Using a Plane-Wave Basis Set. *Comp Mater Sci* **1996**, *6*, 15-50.

27. Blochl, P. E., Projector Augmented-Wave Method. *Phys Rev B* **1994**, *50*, 17953-17979.

28. Perdew, J. P.; Burke, K.; Ernzerhof, M., Generalized Gradient Approximation Made Simple. *Phys Rev Lett* **1996**, *77*, 3865-3868.

29. Andersson, D. A.; Stanek, C. R., Mixing and Non-Stoichiometry in Fe-Ni-Cr-Zn-O Spinel Compounds: Density Functional Theory Calculations. *Phys Chem Chem Phys* **2013**, *15*, 15550-15564.

30. Blochl, P. E.; Jepsen, O.; Andersen, O. K., Improved Tetrahedron Method for Brillouin-Zone Integrations. *Phys Rev B* **1994**, *49*, 16223-16233.

31. Borhan, A. I.; Slatineanu, T.; Iordan, A. R.; Palamaru, M. N., Influence of Chromium Ion Substitution on the Structure and Properties of Zinc Ferrite Synthesized by the Sol-Gel Auto-Combustion Method. *Polyhedron* **2013**, *56*, 82-89.

32. Khalaf, K. A. M.; Al Rawas, A. D.; Gismelssed, A. M.; Al Jamel, A.; Al Ani, S. K. J.; Shongwe, M. S.; Al Riyami, K. O.; Al Alawi, S. R., Influence of of Cr

Substitution on Debye-Waller Factor and Related Structural Parameters of $ZnFe_{2-x}Cr_xO_4$ Spinels. *J Alloy Compd* **2017**, *701*, 474-486.

33. Preisinger, M.; Krispin, M.; Rudolf, T.; Horn, S.; Strongin, D. R., Electronic Structure of Nanoscale Iron Oxide Particles Measured by Scanning Tunneling and Photoelectron Spectroscopies. *Phys Rev B* **2005**, *71*, 165409.

34. Yamashita, T.; Hayes, P., Analysis of XPS Spectra of Fe^{2+} and Fe^{3+} Ions in Oxide Materials. *Appl Surf Sci* **2008**, *254*, 2441-2449.

35. Hosseini, S. A.; Alvarez-Galvan, M. C.; Fierro, J. L. G.; Niaei, A.; Salari, D., MCr_2O_4 (M = Co, Cu, and Zn) Nanospinels for 2-Propanol Combustion: Correlation of Structural Properties with Catalytic Performance and Stability. *Ceram Int* **2013**, *39*, 9253-9261.

36. Lim, C. S.; Chua, C. K.; Sofer, Z.; Klimova, K.; Boothroyd, C.; Pumera, M., Layered Transition Metal Oxyhydroxides as Tri-Functional Electrocatalysts. *J Mater Chem A* **2015**, *3*, 11920-11929.

37. Lian, L.; Hou, L. R.; Zhou, L.; Wang, L. S.; Yuan, C. Z., Rapid Low-Temperature Synthesis of Mesoporous Nanophase $ZnFe_2O_4$ with Enhanced Lithium Storage Properties for Li-Ion Batteries. *Rsc Adv* **2014**, *4*, 49212-49218.

38. Xi, L. F.; Bassi, P. S.; Chiam, S. Y.; Mak, W. F.; Tran, P. D.; Barber, J.; Loo, J. S. C.; Wong, L. H., Surface Treatment of Hematite Photoanodes with Zinc Acetate for Water Oxidation. *Nanoscale* **2012**, *4*, 4430-4433.

39. Wang, H. Y.; Hung, S. F.; Chen, H. Y.; Chan, T. S.; Chen, H. M.; Liu, B., In Operando Identification of Geometrical-Site-Dependent Water Oxidation Activity of Spinel Co_3O_4. *J Am Chem Soc* **2016**, *138*, 36-39.

40. Zhou, Y.; Sun, S. N.; Xi, S. B.; Duan, Y.; Sritharan, T.; Du, Y. H.; Xu, Z. C. J., Superexchange Effects on Oxygen Reduction Activity of Edge-Sharing $[Co_xMn_{1-x}O_6]$ Octahedra in Spinel Oxide. *Adv Mater* **2018**, *30*, 1705407.

41. Newville, M., Fundamentals of XAFS. *Rev Mineral Geochem* **2014**, *78*, 33-74.

42. Akhtar, M. J.; Nadeem, M.; Javaid, S.; Atif, M., Cation Distribution in Nanocrystalline $ZnFe_2O_4$ Investigated Using X-Ray Absorption Fine Structure Spectroscopy. *J Phys-Condens Mat* **2009**, *21*, 405303.

43. Chen, S. M.; Wu, Y. F.; Cui, P. X.; Chu, W. S.; Chen, X.; Wu, Z. Y., Cation Distribution in $ZnCr_2O_4$Nanocrystals Investigated by X-Ray Absorption Fine Structure Spectroscopy. *J Phys Chem C* **2013**, *117*, 25019-25025.

44. Shannon, R. D., Revised Effective Ionic-Radii and Systematic Studies of Interatomic Distances in Halides and Chalcogenides. *Acta Crystallogr A* **1976**, *32*, 751-767.

45. Beverskog, B.; Puigdomenech, I., Revised Pourbaix Diagrams for Chromium at 25-300 °C. *Corros Sci* **1997**, *39*, 43-57.

46. Bajdich, M.; Garcia-Mota, M.; Vojvodic, A.; Norskov, J. K.; Bell, A. T., Theoretical Investigation of the Activity of Cobalt Oxides for the Electrochemical Oxidation of Water. *J Am Chem Soc* **2013**, *135*, 13521-13530.

47. Lutfalla, S.; Shapovalov, V.; Bell, A. T., Calibration of the DFT/GGA+U Method for Determination of Reduction Energies for Transition and Rare Earth Metal Oxides of Ti, V, Mo, and Ce. *J Chem Theory Comput* **2011**, *7*, 2218-2223.

48. Singh, N.; Rhee, J. Y., Electronic Structures and Optical Properties of Spinel $ZnCr_2O_4$. *J Korean Phys Soc* **2010**, *57*, 1233-1237.

49. Guo, X.; Zhu, H. J.; Si, M. S.; Jiang, C. J.; Xue, D. S.; Li, Q., Tuning the Composition of Zn-Fe-O Nanotube Arrays: From Zinc Ferrite $ZnFe_2O_4$ to Hematite α-Fe_2O_3. *Crystengcomm* **2013**, *15*, 8306-8313.

50. Mousavi, Z.; Soofivand, F.; Esmaeili-Zare, M.; Salavati-Niasari, M.; Bagheri, S., Zncr2o4 Nanoparticles: Facile Synthesis, Characterization, and Photocatalytic Properties. *Sci Rep-Uk* **2016**, *6*, 20071.

51. Xu, Z. J., From Two-Phase to Three-Phase: The New Electrochemical Interface by Oxide Electrocatalysts. *Nano-Micro Letters* **2018**, *10*, 8.

52. Chen, D. J.; Chen, C.; Baiyee, Z. M.; Shao, Z. P.; Ciucci, F., Nonstoichiometric Oxides as Low-Cost and Highly-Efficient Oxygen Reduction/Evolution Catalysts for Low-Temperature Electrochemical Devices. *Chem Rev* **2015**, *115*, 9869-9921.

53. Man, I. C.; Su, H. Y.; Calle-Vallejo, F.; Hansen, H. A.; Martinez, J. I.; Inoglu, N. G.; Kitchin, J.; Jaramillo, T. F.; Norskov, J. K.; Rossmeisl, J., Universality in Oxygen Evolution Electrocatalysis on Oxide Surfaces. *Chemcatchem* **2011**, *3*, 1159-1165.

54. Rossmeisl, J.; Qu, Z. W.; Zhu, H.; Kroes, G. J.; Norskov, J. K., Electrolysis of Water on Oxide Surfaces. *J Electroanal Chem* **2007**, *607*, 83-89.

55. Grimaud, A.; Diaz-Morales, O.; Han, B. H.; Hong, W. T.; Lee, Y. L.; Giordano, L.; Stoerzinger, K. A.; Koper, M. T. M.; Shao-Horn, Y., Activating Lattice Oxygen Redox Reactions in Metal Oxides to Catalyse Oxygen Evolution. *Nat Chem* **2017**, *9*, 457-465.

56. Hong, W. T.; Stoerzinger, K. A.; Lee, Y. L.; Giordano, L.; Grimaud, A.; Johnson, A. M.; Hwang, J.; Crumlin, E. J.; Yang, W. L.; Shao-Horn, Y., Charge-Transfer-Energy-Dependent Oxygen Evolution Reaction Mechanisms for Perovskite Oxides. *Energ Environ Sci* **2017**, *10*, 2190-2200.

57. Suntivich, J.; Gasteiger, H. A.; Yabuuchi, N.; Nakanishi, H.; Goodenough, J. B.; Shao-Horn, Y., Design Principles for Oxygen-Reduction Activity on Perovskite Oxide Catalysts for Fuel Cells and Metal-Air Batteries. *Nat Chem* **2011**, *3*, 546-550.

1
2
3
4
5
6
7
8
9
10
11
12
13
14
15
16
17
18
19
20
21
22
23
24
25
26
27
28
29
30
31
32
33
34
35
36
37
38
39
40
41
42
43
44
45
46
47
48
49
50
51
52
53
54
55
56
57
58
59
60

TOC Graphic